Supporting Information: Hybridization of the A- and B-Exciton in a WS_2 Monolayer Mediated by the Transverse Electric Polarized Wave Supported by a Si_3N_4/Ag Heterostructure

Weichen He,[†,§] Shimei Liu,[†,§] Jingting Liu,[†] Shulei Li,[†,‡] Fu Deng,[¶] Haiying Liu,[†] Haihua Fan,[†] Jun Dai,[‡] and Sheng Lan[*,†]

†*Guangdong Provincial Key Laboratory of Nanophotonic Functional Materials and Devices, School of Information and Optoelectronic Science and Engineering, South China Normal University, Guangzhou 510006, China*

‡*School of Optoelectronic Engineering, Guangdong Polytechnic Normal University, Guangzhou 510665, China*

¶*Department of Physics, The Hong Kong University of Science and Technology, Hong Kong 999077, China*

§*These authors contributed equally to this work.*

E-mail: slan@scnu.edu.cn

S1 Numerical simulation settings in COMSOL and FDTD

For the numerical simulations carried out by using COMSOL, we employed the wave optics module and performed the calculations in the frequency domain. The structure was illuminated by a plane wave linearly polarized along the y-axis with an incident angle θ. The purpose of using prism coupling is to satisfy the matching condition of the wave vector by increasing the wave vector of the incident light in free space through the refractive index of the prism. Since the refractive index of the prism is approximately equal to that of the substrate (i.e., $n_{\mathrm{prism}} = n_{\mathrm{SiO_2}}$), the use of prism coupling is equivalent to the plane wave generated directly in the SiO_2 substrate with an incident angle θ, as shown in Figure S1.

We adopted a standard two-step process for simulating the scattering spectra of an Au nanorod placed on the Si_3N_4/Ag and WS_2/Si_3N_4/Ag heterostructures. In the first step, the full field was calculated with the absence of Au nanorod and used as the background field for the next step. In this step, Floquet boundary conditions (periodic boundary conditions) were applied in the x- and y-directions while two port boundary conditions were applied in the z-direction. One port was used for generated incident plane wave and absorbed reflection wave, while the other port was used for the absorbed transmitted wave. In the second step, the scattered field was calculated in the presence of the Au nanorod and using the background field in the first step as source to determine the scattering induced by the Au nanorod. In this step, the structure was enclosed by a perfectly matched layer (PML) that absorbed completely the outgoing wave and the scattering intensity was calculated by integrating the Poynting vector of the scattered field over a cuboid surface enclosing the structure.

In order to improve the efficiency of the numerical simulation, the reflection spectra of the Si_3N_4/Ag and WS_2/Si_3N_4/Ag heterostructure were performed in a two-dimensional structure with Floquet boundary conditions in the x-direction and port boundary conditions as well as PML in the z-direction.

For the numerical simulations carried out by using FDTD, a dipole source was placed at

various positions within the WS_2 monolayer to simulate exciton behavior. The simulation of radiation intensity was also performed using a standard two-step process, initially in the absence of the Au nanorod and subsequently with the Au nanorod. Thus, the actual radiation intensity is obtained by subtracting the result of the first calculation from that of the second one. A power monitor with a diameter of 750 nm, corresponds to the collection area of the objective used in the experiment (NA = 0.7), was placed on top of Au nanorod to detect the radiation emitted by it. The entire structure was enclosed by a PML to completely absorb the outgoing wave.

For the numerical simulations performed by using COMSOL, free tetrahedron meshes were employed in the simulation region while cuboid meshes were used in the PML. In comparison, Yee grids were used in the numerical simulations based on FDTD. The mesh sizes used for the WS_2 monolayer and Au nanorod were set to be 0.5 and 1.0 nm in both simulation methods to ensure the convergence of the numerical simulations. The mesh size for the remaining parts of the structure was automatically generated by the software, using extra fine element size in COMSOL and mesh accuracy setting of 4 in FDTD.

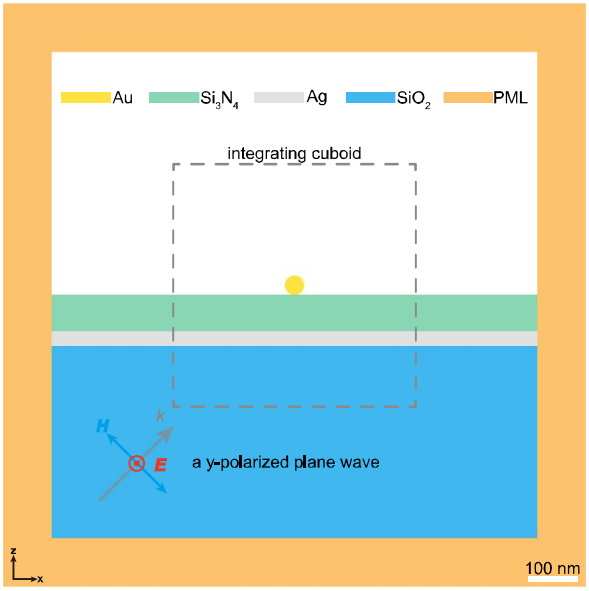

Figure S1: Schematic showing the simulation model used to excite the TE wave by using a linearly plane wave and the scattering intensity is calculated by integrating over a cuboid surface that encloses the Au nanorod in COMSOL.

S2 Expression for the amplitude in the Coupled Oscillator Model

In the Coupled Oscillator Model section of the main text, we present the steady-state equations, which can be succinctly expressed in matrix form as follows:

$$\begin{pmatrix} \alpha_{\mathrm{TE}} & 2j\omega g_{\mathrm{TE-A}} & 2j\omega g_{\mathrm{TE-B}} & 0 \\ -2j\omega g_{\mathrm{TE-A}} & \alpha_{\mathrm{A}} & 0 & 2j\omega g_{\mathrm{LSPR-A}} \\ -2j\omega g_{\mathrm{TE-A}} & 0 & \alpha_{\mathrm{B}} & 0 \\ 0 & -2j\omega g_{\mathrm{LSPR-A}} & 0 & \alpha_{\mathrm{LSPR}} \end{pmatrix} \begin{pmatrix} x_{\mathrm{TE}} \\ x_{\mathrm{A}} \\ x_{\mathrm{B}} \\ x_{\mathrm{LSPR}} \end{pmatrix} = \begin{pmatrix} F_{\mathrm{TE}} \\ 0 \\ 0 \\ F_{\mathrm{LSPR}} \end{pmatrix}, \tag{S1}$$

where the coefficients α_m (m = TE, A, B, and LSPR) are defined as:

$$\begin{cases} \alpha_{\mathrm{TE}} = \omega_{\mathrm{TE}}^2 - j\omega\gamma_{\mathrm{TE}} - \omega^2 \\ \alpha_{\mathrm{A}} = \omega_{\mathrm{A}}^2 - j\omega\gamma_{\mathrm{A}} - \omega^2 \\ \alpha_{\mathrm{B}} = \omega_{\mathrm{B}}^2 - j\omega\gamma_{\mathrm{B}} - \omega^2 \\ \alpha_{\mathrm{LSPR}} = \omega_{\mathrm{LSPR}}^2 - j\omega\gamma_{\mathrm{LSPR}} - \omega^2 \end{cases}. \tag{S2}$$

In fact, Eq. S1 are the system of linear equations. By employing Cramer's rule to solve this system of linear equations, we derive the amplitudes of the TE wave and LSPR:

$$x_{\mathrm{TE}} = F_{\mathrm{TE}} \left(\frac{\alpha_{\mathrm{A}}\alpha_{\mathrm{B}}\alpha_{\mathrm{LSPR}} - 4\alpha_{\mathrm{B}} g_{\mathrm{LSPR-A}}^2 \omega^2}{\Delta} \right) - F_{\mathrm{LSPR}} \left(\frac{4\alpha_{\mathrm{B}} g_{\mathrm{TE-A}} g_{\mathrm{LSPR-A}} \omega^2}{\Delta} \right), \tag{S3}$$

$$x_{\mathrm{LSPR}} = -F_{\mathrm{TE}} \left(\frac{\alpha_{\mathrm{TE}} g_{\mathrm{TE-A}} g_{\mathrm{LSPR-A}} \omega^2}{\Delta} \right) + F_{\mathrm{LSPR}} \left(\frac{\alpha_{\mathrm{TE}}\alpha_{\mathrm{A}}\alpha_{\mathrm{B}} - 4\alpha_{\mathrm{B}} g_{\mathrm{TE-A}}^2 \omega^2 - 4\alpha_{\mathrm{A}} g_{\mathrm{TE-B}}^2 \omega^2}{\Delta} \right), \tag{S4}$$

where Δ is the determinant of the coefficient matrix in Eq. S1, given by: $\Delta = \alpha_{\mathrm{TE}}\alpha_{\mathrm{A}}\alpha_{\mathrm{B}}\alpha_{\mathrm{LSPR}} - 4\alpha_{\mathrm{B}}\alpha_{\mathrm{LSPR}} g_{\mathrm{TE-A}}^2 \omega^2 - 4\alpha_{\mathrm{A}}\alpha_{\mathrm{LSPR}} g_{\mathrm{TE-B}}^2 \omega^2 - 4\alpha_{\mathrm{TE}}\alpha_{\mathrm{B}} g_{\mathrm{LSPR-A}}^2 \omega^2 + 16 g_{\mathrm{TE-B}}^2 g_{\mathrm{LSPR-A}}^2 \omega^4$.

S3 Influence of the thickness of the Ag film on the TE wave

We investigated the influence of the thickness of the Ag film on the TE wave excited on the Si_3N_4/Ag heterostructure. The evolution of the reflection spectra of the incident wave from the Si_3N_4/Ag heterostructure with increasing the thickness of the Ag film is presented in Figure S2. The incident angle was chosen to be $\theta = 48°$. It is noticed that the reflection dip corresponding to the resonant wavelength of the TE wave exhibits a redshift when the thickness of the Ag film is reduced. In addition, the linewidth of the TE wave is significantly broadened when the thickness of the Ag film becomes smaller than 30 nm.

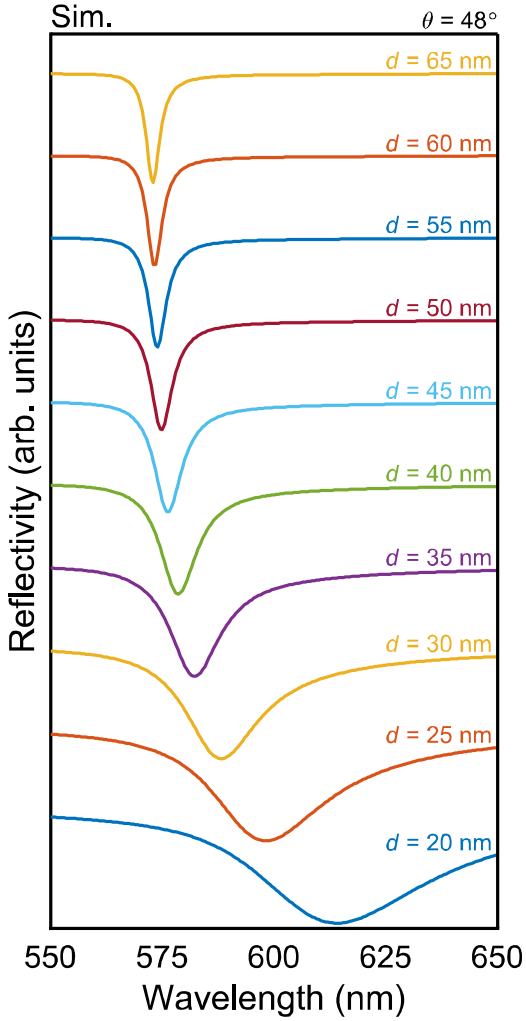

Figure S2: Reflection spectra calculated for Si_3N_4/Ag heterostructures composed of Ag films with different thicknesses.

S4 Determining the optimum configuration for the Si_3N_4/Ag heterostructure

We calculated the two-dimensional reflection spectra for Si_3N_4/Ag heterostructures with different thickness of the Si_3N_4 layer, as shown in Figure S3. Here, thickness of the Ag film was fixed at $d = 50\,\text{nm}$ and incident angle was set at $\theta = 48°$. A linear relationship between the resonant wavelength of the TE wave and thickness of the Si_3N_4 layer is observed. The thickness of the Si_3N_4 layer has little influence on the linewidth of the TE wave. Basically, the resonant wavelength of the TE wave can be tuned across the visible light spectra by varying either the thickness of the Si_3N_4 layer or the incident angle. For the Si_3N_4/Ag heterostructure with a 75 nm-thick Si_3N_4 layer, the resonant wavelength of the TE wave is located on the short-wavelength side of the A-exciton when the incident angle is just above the critical angle. Therefore, we think 75 nm is a suitable thickness for the Si_3N_4 layer.

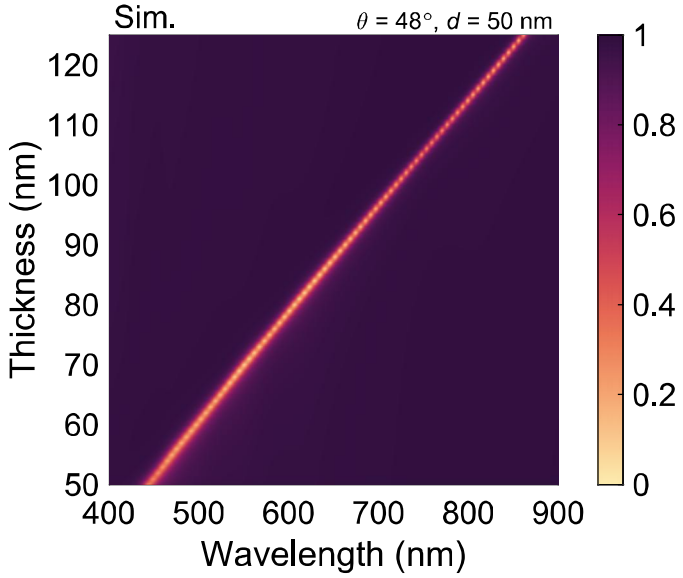

Figure S3: Two-dimensional reflection spectra calculated for the Si_3N_4/Ag heterostructure with different thickness of the Si_3N_4 layer. Here, the thickness of Ag film is fixed at $d = 50\,\text{nm}$ and the incident angle is set at $\theta = 48°$.

In Figure S4, we calculated the reflection spectra for the Si_3N_4/Ag heterostructures composed of Ag films with different thicknesses. In each case, the incident angle is intentionally